

Mechanical action of the transverse spin momentum of an evanescent wave on gold nanoparticles in biological objects media

O. V. ANGELSKY, C. YU. ZENKOVA*, D. I. IVANSKY
Chernivtsy National University, Chernivtsy, Ukraine

The theoretical and experimental confirmation of the existence of a transverse spin momentum in an evanescent wave excited above the surface of a birefringent biological section is suggested in this research work. The possibility of controlling gold nanoparticles by the vertical spin of an evanescent wave in a surrounding fluid of tissue near the surface layer of the section is demonstrated.

(Received January 10, 2018; accepted June 7, 2018)

Keywords: Evanescent wave, Nanoparticles, Biotissue

1. Introduction

Nanotechnology is widely used in biomedicine, including nanotherapy, transportation of medical products, biomarking, cancer diagnosis, bioprobng. All this is based on the use of non-invasive methods for evaluating and analyzing pathological changes in tissues with the search for new opportunities for treating diseases and possible pathologies by non-traumatic, easily accessible methods.

One possible application of molecular nanotechnology can be realized in nanomedicine, a developing approach dedicated to the creation of microscopic biomedical devices, such as nanomachines and nanorobots. Photon nanoscale devices act as vehicles for the transfer and delivery of therapeutic agents, and serve as detectors for a particular type of disease [1]. As a rule, such medical robots are programmed to perform certain functions and are managed outside the human body. In this case, drugs are injected into nanoparticles, which imply side effects reduction, thereby overcoming the problems of solubility and toxicity.

Thus, in particular, gold nanoparticles measuring 50 to 80 nm in size are effectively used [1, 2]. These particles, being non-toxic to the body, can be introduced into the body in order to detect and destroy pathologically altered tissues in a non-invasive manner. For transportation of medicines to certain parts of the body, the appropriately prepared nanocoating [1] is also successfully used.

In this connection, evanescent waves are of particular interest, as they being limited by the size of thin layers propagate along the surface and are able to transmit their own angular momentum to the nanoparticles localized on the surface, thus setting a certain direction of their displacement.

Recent studies [3-5] of evanescent waves excited by linearly polarized waves of different azimuth demonstrate the possibility of realizing the transverse spin momentum

in the plane above the section surface. For a linearly polarized wave with 45° polarization azimuth, falling on the interface of two media, the so-called vertical spin of the evanescent wave arises at an angle that ensures total internal reflection (TIR) [5]. It is worth mentioning that by changing the incidence angle of light to the interface, it is possible to control the direction of the motion of nanoparticles, and, accordingly, of the entire nanostructure, which, depending on the problem being solved, can be a combination of different constituent components.

The aim of this work is to search for optimal conditions for the formation of the vertical spin of the evanescent wave to control the mechanical displacements of gold nanosized particles localized on the surface of a section of a biological birefringent substance. We will assume that the medium, in which the evanescent wave is excited, is close in composition to a physiological one. It is proposed to use the so-called tissue fluid, which is based on water, amino acids, fatty acids, hormones and various waste cells, the dimensions of which are much smaller as compared with controlled gold nanoparticles. As a sample, a birefringent medium is selected, in which macroscopic anisotropy is caused by the fibrillar structure of partially oriented close-packed fibers [8]. Muscle tissue, tendon and derma, i.e. biotissues are the examples of such tissues.

According to its properties, the biotissue may be isotropic or exhibits the properties of uniaxial or biaxial crystals [6,9]. Any changes that lead to abnormal tissue growth contribute to a change in optical properties, for example, formation of isotropic media.

For a biotissue, in particular, muscle fiber, the derma thickness usually amounts to about 50-100 μm . For some other organs, the thickness may be about 300 μm . Such thickness values ensure the coherence and polarization of laser radiation as it penetrates deep into the structure [8]. It is this fact that allows probing of the selected medium by

polarized radiation. Moreover, choosing the wavelength of the laser radiation within the "transparency window" (800-1500 nm) [8] for biological tissues enables to achieve the total internal reflection at the biotissue-liquid interface. And this means it is possible to realize the vertical spin of an evanescent wave with further transportation of gold nanoparticles in the chosen direction.

2. Model of optical anisotropy of biological tissues

The optical anisotropy of the tissue is determined by the structural characteristics and the difference between the refractive indices of collagen fibers and the base material [10]. Using a two-component model with the representation of collagen fibers in the form of long cylinders [11], optical anisotropy Δn can be characterized as

$$\Delta n = \frac{(n_{col}^2 - n_{bas}^2)(n_{col} + n_{bas})c(1-c)}{(1+c)n_{col}^2 + (1-c)n_{bas}^2},$$

where c is the volume fraction of collagen fibers, n_{col} , n_{bas} – refractive indices for collagen and the base material respectively. Collagen has refractive index of 1.45, and is immersed in a dielectric medium with the refractive index of 1.37. Calculation of the refractive indices of ordinary (n_o) and extraordinary (n_e) rays in an anisotropic biotissue medium was carried out in the approximation of the model of parallel dielectric cylinders uniformly distributed in the interval from 80 to 120 nm with a volume fraction of cylinders equal to $f = 0.8$ and a radius of 50 nm, which is close to typical morphological parameters characterizing the fibrillar structure of the derma [12]. Forming a denser packing of cylinders, i.e. realizing the model of a practically homogeneous medium, the scattering in the volume of the model section is reduced to minimum. Then, for an anisotropic, practically homogeneous medium [13,14], the orientation of the fast axis coincides with that of the collagen fibers of the muscle fiber.

To avoid the destruction of biological tissue when heated by laser radiation, it is necessary to select both the duration of the radiation pulse (the duration of the radiation exposure to minimize the damage zone and irreversible temperature changes) and the temperature interval of tissue heating [15-17]. For a laser with a depth of penetration into biological tissue up to 1 mm, the pulse duration is chosen to be approximately 1 μ s, which provides the temperature of heating the biological tissue to 50-600, while the optical properties of the tissue do not change.

According to [12], the refractive indices of ordinary and extraordinary beams are estimated as

$$n_o = \sqrt{\varepsilon_o} = \sqrt{\varepsilon_{bas} \left(1 + \frac{2\alpha f}{1 - \alpha f}\right)}$$

$$n_e = \sqrt{\varepsilon_e} = \sqrt{\varepsilon_{col} f + \varepsilon_{bas} (1 - f)},$$

where $\alpha = \frac{\varepsilon_{col} - \varepsilon_{bas}}{\varepsilon_{col} + \varepsilon_{bas}}$ – polarization ability of dielectric cylinders.

The simulation was carried out in the approximation when the vector of electric field intensity propagating in a medium of a linearly polarized monochromatic electromagnetic wave with unit amplitude was oriented parallel or perpendicular to the axes of the cylinders, respectively [12]. The applied approach is based on using of the criterion for the equality of the energy of the electromagnetic field in the volume of the medium occupied by the model scattering center and the field energy in the equivalent volume of a spatially homogeneous medium [12].

3. Analysis of the mechanism of the vertical spin excitation in the near-surface layer of tissue fluid

The evanescent wave, caused by the complete internal reflection of a linearly polarized wave of 45° azimuth at the interface "biotissue-liquid (water)", is elliptically polarized, and the ellipticity is determined by the direction of propagation of the beam in the biotissue medium.

Let us consider the conditions for the formation of the vertical spin of the evanescent wave. Fig. 1 shows the spreading of an optical flat parallel beam through a model section of the birefringent medium of a biotissue.

We will assume that the optical force produced by an elliptically polarized beam that propagates in the direction towards the interface "birefringent section-tissue fluid" (\vec{F}_{br12}), and the force acting in the opposite direction (\vec{F}_{br21}) are compensated. It was the case when the incidence angle of the beam on the section was determined, and the corresponding azimuth of the beam polarization at the input was selected in order to form the transverse polarization-dependent force of the evanescent wave.

Further we will use here the following terminology: the beam impinging on the first surface of the slice will be referred to as a probing beam, while the beam impinging on the second surface – the incident beam.

Let us estimate the magnitude of the optical force for an elliptically polarized beam, which propagates in the birefringent section of the biotissue [5]. In the general case, for a plane elliptically polarized wave of circular frequency ω [18], the optical force can be represented as the time-averaged Maxwell stress tensor \vec{T} by integrating of the whole spatial element with consideration of the beam aperture r :

$$\vec{F}^D = \int \langle \vec{T} \rangle \hat{n} d^2 r, \quad (1)$$

where

$$\langle \overset{\text{P}}{T}_{ij} \rangle = [\varepsilon_0 \overset{\text{P}}{E}_i \otimes \overset{\text{P}}{E}_j + \frac{1}{\mu_0} \overset{\text{P}}{B}_i \otimes \overset{\text{P}}{B}_j - \frac{1}{2} (\varepsilon_0 |\overset{\text{P}}{E}|^2 + \frac{1}{\mu_0} |\overset{\text{P}}{B}|^2) I]$$

According to the figure, $i, j = y, z$; \otimes is the dyadic product, I is the unit matrix, \hat{n} is the surface-normal

vector, $B = \sqrt{\varepsilon \varepsilon_0} E$ is the magnetic inductance vector, and ε is the media permittivity.

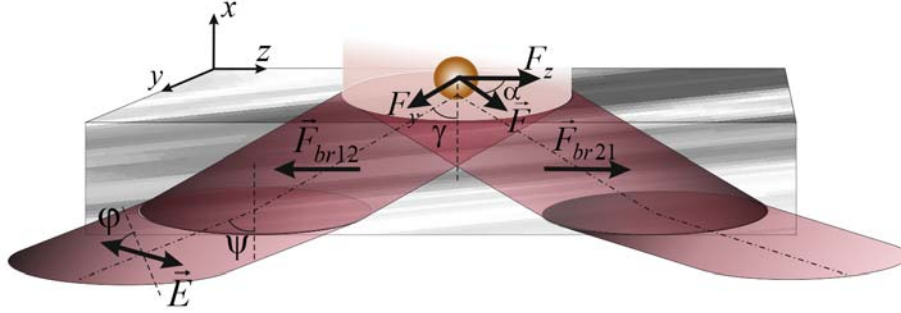


Fig.1. Scheme showing the propagation of a beam through the birefringent section of biotissue during the formation of vertical spin of an evanescent wave above the surface of the section. Here, φ – the azimuth of polarization of the probing beam, ψ – the angle of incidence of the probing beam, γ – the angle determining the propagation direction of the incident beam. $\overset{\text{P}}{F}_{br12}$ – optical force directed to the external surface of the section and $\overset{\text{P}}{F}_{br21}$ – optical force acting in the opposite direction. F_y, F_z – the components of the optical force $\overset{\text{P}}{F}$ determined by the action of the evanescent wave on the gold particles above the surface of the section, the resultant of which determines the direction of the particles motion (α)

In general, taking into account the optical path difference and the direction of beam propagation in the model section γ , the electrical vector of an incident elliptically polarized wave:

$$\overset{\text{P}}{E}_{inc12} = \begin{pmatrix} 0 \\ E_y (\cos \Theta \cos \Phi + i \sin \Phi \cos \Theta) \exp(ikn_o d / \cos \gamma) \\ E_z (\cos \Theta \cos \Phi - i \sin \Phi \cos \Theta) \exp(ikn'_e d / \cos \gamma) \end{pmatrix} \times \exp i(kkx d / \cos \gamma - \omega t) \quad (2)$$

Here Φ is the degree of ellipticity of the polarization [19] defined as tangent of the ratio of the minor to major axes of an ellipse, and k is the free-space wavenumber, κ – extinction coefficient ($m = n + i\kappa$ (for birefringence $n(n_o, n_e)$)).

Here

$$E_y = E_0 \sin \varphi (\cos \theta \cos \varphi + \sin \theta \sin \varphi), \\ E_z = E_0 \cos \varphi \cos \psi (\sin \theta \cos \varphi - \cos \theta \sin \varphi) -$$

orthogonal components of linearly polarized beam with the azimuth φ , θ – angle between the main axis of the section and the direction of the electric field vector of the probing beam, ψ is the incidence angle of the probing beam.

While falling onto the second cut surface, the beam undergoes total internal reflection. The phase shift $\delta = \delta_p - \delta_s$ between the orthogonal components in the reflected beam is determined by the angle of the beam incidence on the second surface of a section.

In this case, the electric vector of the reflected wave can be represent

$$\overset{\text{P}}{E}_{inc21} = \begin{pmatrix} 0 \\ E_y (\cos \Theta \cos \Phi + i \sin \Phi \sin \Theta) \exp(i(2kn_o d / \cos \gamma + \delta)) \\ E_z (\sin \Theta \cos \Phi - i \cos \Theta \sin \Phi) \exp(i(2kn'_e d / \cos \gamma)) \end{pmatrix} \times \exp i(kkx d / \cos \gamma - \omega t) \quad (3)$$

The absence of the torsion torque in a linearly polarized wave assumes the calculation of optical forces without taking into account the rotational motions of the sample, which is the basis for calculating the optical forces in the sample and determining the conditions enabling to realize the vertical spin.

According to (1), taking into account (2) and (3), we calculate the optical force for both beams propagating in two different directions – towards the upper surface of the section and in the opposite direction, which is determined by the condition of total internal reflection on this surface. Next, we determine the set of parameters under which these forces are compensated. When the vertical spin is realized, for the described conditions, the evanescent wave

above the interface will be elliptically polarized, with the maximal values of the polarization components in the orthogonal directions. In this case, the manifestation of the transverse component of the optical force of the evanescent wave becomes obvious.

Fig. 2 shows the results of modeling situations in which the optical force due to the beam propagating

toward the outer surface of the section compensates the optical force produced by the reflected beam. Changing the angle of incidence ψ of the probing beam for different section thickness d , the polarization azimuth φ of this beam is selected, when the compensation of the optical forces (F_{br12}, F_{br21}) becomes possible.

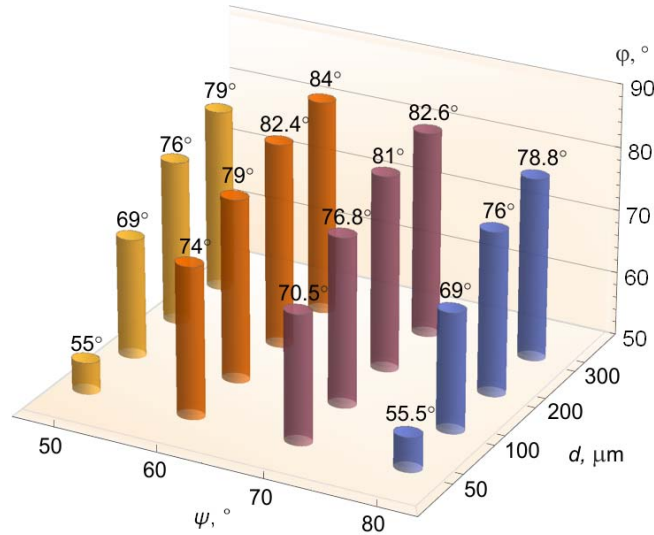


Fig. 2. The constructed histogram is based on the condition of the optical forces (F_{br12}, F_{br21}) compensation at propagation of an elliptically polarized beam to the outer surface of the birefringent section and in the direction specified by the complete internal reflection. Here d is the thickness of the section, ψ – the incidence angle of the probing beam, φ – the polarization azimuth of the probing beam. The height of the columns corresponds to the value of polarization azimuth of the probing beam

Among the possible options for compensating the optical force in the volume of a biological section (Fig. 2), we choose the optimal one, concerning its experimental implementation. It can be shown that obtaining the polarization azimuth of the incident wave at 45° at the ‘section-tissue fluid’ interface is realized when the incidence angle of a linearly polarized probing beam on the first surface of the section with the polarization azimuth of 79° is about 60° for the thickness of the section $100 \mu\text{m}$ respectively. These parameters of the probing beam ensure complete internal reflection on the external surface of the section and the realization of an evanescent wave above the interface. This choice of parameters enables to experimentally visualize the transverse motion of gold particles in the surface layer of the tissue fluid, given by an evanescent wave.

The linearly polarized beam in the birefringent material is transformed into an elliptically polarized one and, as it propagates through the medium, the parameters of the polarization ellipse change [20-22]. The formation of an elliptically polarized wave is accompanied by the appearance of a spin angular momentum. At that, an optical force is generated, the cause of which consists in the change of the density of the spin moment of the propagating beam. As a consequence, the overall distribution of forces in the section can vary. However, the effect of this optical force is reduced to a minimum if the

section is stationary. In the real conditions of the existence of biological tissues, reproduced in the experiment suggested in the work, the need to evaluate this optical force is no longer significant.

Thus, an evanescent wave, being excited above the interface, can be described by the following equation [23]

$$\vec{E}_{ev} = E \begin{pmatrix} \frac{1}{\sqrt{1+|m|^2}} \\ \frac{m}{\sqrt{1+|m|^2}} \frac{k}{k_z} \\ -i \frac{1}{\sqrt{1+|m|^2}} \frac{\kappa}{k_z} \end{pmatrix} \exp(-\kappa x) \exp(i(k_z z - \omega t))$$

Here $k_z = k \frac{n_o}{n} \sin \gamma$, $\kappa = k \sqrt{\left(\frac{n_o}{n}\right)^2 \sin^2(\gamma) - 1}$ is the

exponential decay rate, $m = \frac{T_{\perp}}{T_{\parallel}} m_1$ is the polarization state

of an evanescent wave [4], where m_1 is the polarization state of the probing beam impinging on the interface plate-air being equal to unity for linear polarization with

the azimuth of polarization 45° , γ is the incidence angle on the surface, where TIR takes place.

The electrical strength of the field of an evanescent wave is $E = \frac{k_z}{k} \sqrt{\frac{\mu_1}{\mu}} TE_0$, where

$$T = \frac{\sqrt{|T_{//}|^2 + |m_1|^2 |T_{\perp}|^2}}{\sqrt{1 + |m_1|^2}} \exp[i \arg T_{//}]$$

is the transmission coefficient [4], and $T_{//}$, T_{\perp} are the Fresnel transmission coefficients.

The values of the optical force due to the evanescent wave in this experiment are not significant, since the controlled motion of particles by the evanescent wave in the near-surface layer of the section is of more interest.

We estimate the magnitude of the density of the spin and orbital momentum in the transverse y and longitudinal z directions (Fig. 1), followed by the estimation of the value of the force in the corresponding directions.

The spin momentum density in this case is expressed as [3, 4] $p_s = \frac{1}{16\pi\omega} \nabla \times \text{Im}[\mathbf{E}_{\text{ev}}^* \times \mathbf{E}_{\text{ev}}]$. It has both

longitudinal and transversal components [3]. Thus, the resulting momentum density in the z -direction is given by

$$p_z = p_{oz} + p_{sz} = \frac{A^2}{8\pi\omega} \left[\left(k_z + \frac{m^2 k^2}{k_z} + \frac{\kappa^2}{k_z} \right) - 2 \frac{\kappa^2}{k_z} \right] \exp(-2\kappa x)$$

and the transversal momentum caused by the vertical spin

$$p_y = p_{sy} = \frac{A^2}{4\pi\omega} \frac{k \kappa}{k_z} \text{Im } m \exp(-2\kappa x),$$

$$\text{where } A = E \frac{1}{\sqrt{1 + |m|^2}}.$$

Gold nanoparticles are used as an object of research. Therefore, to calculate the optical force acting on the particles, we use Mie's scattering, in the approximation of which [4] $\mathbf{F} = \int_s \Delta \mathbf{p} dS$, where $\Delta \mathbf{p}$ is the change of

momentum density. Simulation of the force affecting a plate and causing its motion presumes integration over the illuminated area assuming a beam aperture 6° .

The route of the nanoparticle motion is determined by

$$\text{the angle } \alpha = \text{arctg} \frac{F_y}{\sqrt{F_y^2 + F_z^2}}$$

between the Poynting vector propagation along the z axis and the resultant direction of the particle motion, which does not coincide with either the longitudinal (F_z) or the transverse (F_y) directions of the optical force components action.

As modeling results show, it is possible to control the direction of nanoparticles motion due to the choice of the incidence angle of the probing beam on the first section surface (Fig. 3). So, for the chosen incidence angle of 60° , the angle determining the direction of nanoparticles motion is about 11° that is observed in the experiment.

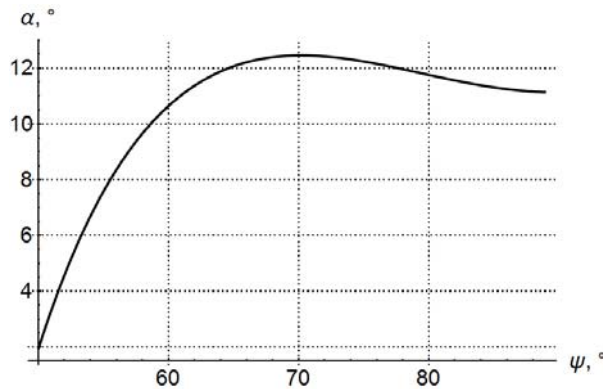


Fig. 3. Dependence of the direction of motion of gold particles in the near-surface layer of the tissue fluid, depending on the change in the incidence angle of the probing beam at thickness of a section of $100 \mu\text{m}$

4. Experimental demonstration of the control of nanoparticles by the vertical spin of the evanescent wave

In general, the control of the nanoparticles motion by a homogeneous evanescent field is hampered by their Brownian motion. However, not the process of capturing particles by the evanescent wave, namely the displacement of the ensemble of nanoparticles by the evanescent field is demonstrated in this research work. Showing such a motion is rather a qualitative than a quantitative

demonstration of the possibilities of using this phenomenon.

The scheme of the experiment is demonstrated in the Fig. 4.

As a radiation source the semiconductor laser 8 (980 nm 4000 mW Laser from Wavespectrum with the ability to control the beam power to 50-100 mW, which ensures the integrity of the biological tissue during irradiation) is used, which was focused on the interface of the section-physiological medium 4 without spatial frequency filtration. The aperture of the beam was 6° .

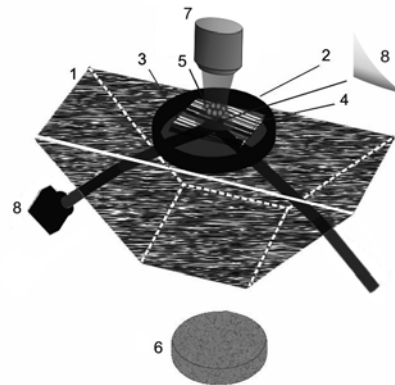


Fig. 4. Scheme of experimental setup for demonstrating controlled motion of gold nanoparticles by an evanescent wave in the near-surface layer of a birefringent section. Here, 1 – prism; 2 – cuvettes with tissue fluid 3; 4 – birefringent section; 5 – gold nanoparticles controlled by evanescent wave 8; 6 – white-light illuminating source; 7 – laser beam provided particle trapping; 8 – laser radiation source producing an evanescent wave

The use of a prism to form a condition for TIR is an alternative to other approaches associated with the use of waveguides, fluorescence technology or microspheres [24–28]. The availability of this optical element determining the simplicity of achieving the necessary conditions for total internal reflection which is accompanied by the evanescent wave creation forms a significant advantage of the experimental realization of the vertical spin.

In the suggested experiment, the focal spot was of the nearly square shape, with a diagonal of about 50 μm .

The experimental conditions allowed regulating the azimuth of the linear polarization of the test and incident beams by rotating the light source. The receiver of the radiation was a 1.3-megapixel CCD camera without a

protective glass, sensitive in the infrared (IR) region. This enabled to study both the particles, using the illumination in the visible region, and the position of the incident IR beam on the section. The radiation intensity of the laser was extracted with the power typical of working with biological objects.

To control the nanoparticles motion it is necessary to avoid the particle's interaction with the anisotropic mechanical environment nearby a solid interface [29]. Using an additional laser source 7 (660-nm laser) provides an optical trapping mechanism with the displacement of particles from the surface. Nonetheless the particles remain in the area of the evanescent wave (Fig. 4, 8) action.

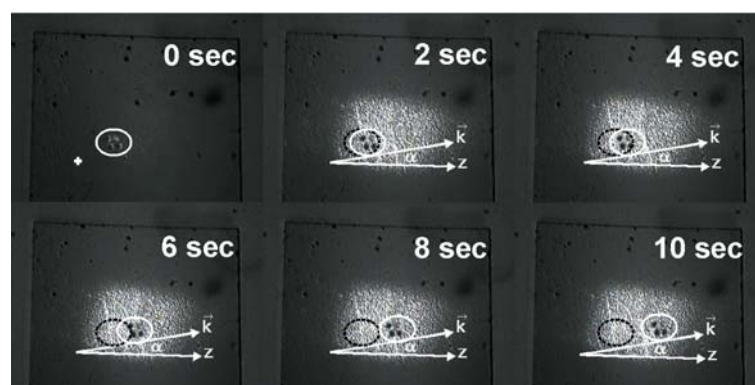


Fig. 5. Photos demonstrating the change of gold nanoparticles about 60 nm size locations by the action of the evanescent wave, produced in the near-surface layer of the tissue: white ellipse notes the position of managed nanoparticles at different moments of time; black ellipse notes the initial position of these particles. α is the angle between directions z and k (vector determining the direction of the resulting optical force F^p action)

To reduce the surface tension of the tissue fluid used in the experiment and to demonstrate the action of the evanescent wave, thin, near-surface layers of fluid were

used with the appropriate selection of the shape and curvature of the liquid meniscus.

The radius of the meniscus was determined by the wettability of the section surface with the fluid and amounted to about 58 nm. On the other hand, the heating of the fluid also presupposed a decrease in the surface tension, which enabled to follow the action of the evanescent wave.

The results of the experiment are presented in the next picture (Fig. 5). The flux of particles entrained by the evanescent wave moved in the transverse direction of the near-surface fluid layer, which is due to deviation from the original horizontal direction of motion. The deflection angle corresponds to the results obtained due to the theoretical approximation and amounts to about 11° . It was possible to approximate the average velocity of particle motion in our experiment that was about of $35 \frac{\mu\text{m}}{\text{s}}$. It is natural to assume that by changing the parameters of the probing beam, we are able to control the movement of nanoparticles in the supersurface layer of the biological object, thereby increasing the possibilities of transporting the dosated portions of drugs to handle pathological biostructures.

5. Conclusions

The possibility of controlling the ensemble of nanosized gold particles with an evanescent wave excited in the surface layer of the surrounding fluid above the birefringent section of biological tissue is demonstrated. Selection of the parameters of the probing beam for which it is possible to realize a vertical spin above the section surface at the total internal reflection on the upper section boundary is proposed. The obtained results enable to expand the potentiality of controlled motion of microdoses of matter in biosystems, which is achieved by laser radiation of appropriate power.

References

- [1] D. M. Sabatini, Nova Science Publishers, New York: 307, 2007.
- [2] C. Yu. Zenkova, M. P. Gorsky, I. V. Soltys, P. O. Angelsky, Ukrainian Journal of Physical Optics **13**(4), 183 (2012).
- [3] M. Antognozzi, C. R. Bermingham, H. Hoerber, M. R. Dennis, A. Ya. Bekshaev, R. L. Harniman, S. Simpson, J. Senior, K. Y. Bliokh, F. Nori, Nature Physics **12**, 731 (2016).
- [4] K. Y. Bliokh, A. Y. Bekshaev, F. Nori, Nature Communications **5**, Article number: 4300 (2014).
- [5] O. V. Angelsky, S. G. Hanson, P. P. Maksimyak, A. P. Maksimyak, C. Yu. Zenkova, P. V. Polyanskii, D. I. Ivanskyi, Optics Express **25**(3), 2299 (2017).
- [6] C. Yu. Zenkova, D. I. Ivanskyi, T. V. Kiyashchuk, Optica Applicata **47** (3), 483 (2017).
- [7] V. V. Tuchin, Successes of Physical Sciences **167**(5), 517 (1997) (in Russian).
- [8] A. G. Ushenko, S. B. Ermolenko, D. N. Burkovets, Yu. A. Ushenko, Optics and Spectroscopy **87**, 434 (1999).
- [9] V. A. Serebryakov, "Laser technologies in medicine", Sn. Petersburg, SP.: SPSU edition, IPMO, 266 p., 2009 (in Russian).
- [10] D. A. Zymnyakov, G. V. Simonenko, V. V. Tuchin, Optical Journal **77**(9), 69 (2010) (in Russian).
- [11] A. Ye. Gryshchenko, "Mechanooptics of polymers", Sn. Petersburg, SP.: SPSU edition, 196 p., 1996 (in Russian).
- [12] D. A. Zymnyakov, Yu. P. Sinichkin, O. V. Ushakova, Quantum Electronics **37**(8), 777 (2007) (in Russian).
- [13] O. V. Angelsky, M. P. Gorsky, S. G. Hanson, V. P. Lukin, I. I. Mokhun, P. V. Polyanskii, P. A. Ryabiy, Optics Express **22**(5), 6186 (2014).
- [14] C. Yu. Zenkova, M. P. Gorsky, P. A. Ryabiy, I. Gruia, Optica Applicata **45**(2), 139 (2015).
- [15] V. N. Vasiliev, S. K. Serkov, Journal of Engineering Physics and Thermophysics **64**(5), 487 (1993) (in Russian).
- [16] M. Jasiński, Journal of Applied Mathematics and Computational Mechanics **14**(4), 67 (2015).
- [17] D. Fedele F. Fusi, Energy for Health, https://www.asalaser.com/sites/default/files/documenti/energy-for-ealth/e4h6_thermal_effects_nir_laser_radiation_10_15.pdf
- [18] C. Rockstuhl, H. P. Herzig, J. Opt. Soc. Am. A **22**, 109 (2005).
- [19] M. E. J. Friese, T.A. Nieminen, N. R. Heckenberg, H. Rubinsztein-Dunlop, Nature **394**, 348 (1998).
- [20] T. Tudor, J. Opt. Soc. Am. A **14**, 2013 (1997).
- [21] O. V. Angelsky, N. N. Dominikov, P. P. Maksimyak T. Tudor, Applied Optics **38**, 3112 (1999).
- [22] C. Yu. Zenkova, Applied Optics **53**(10), B43 (2014).
- [23] A. Hayata, J. P. Balthasar Muellera, F. Capasso, PNAS Early Edition, 5 pages (2015).
- [24] Y. Raichlin, A. Katzir, Applied Spectroscopy **62**(2), 55A (2008).
- [25] A. Maimaiti, V. Giang Truong, M. Sergides, I. Gusachenko, Si'le Nic Chormaic, Scientific Reports **5**: 9077 | DOI: 10.1038/srep09077 (2015).
- [26] S. T. Ross, S. Schwartz, Th. J. Fellers, M. W. Davidson, <https://www.microscopyu.com/techniques/fluorescence/total-internal-reflection-fluorescence-tirf-microscopy>
- [27] G. D. Byrne, M. C. Pitter, J. Zhang, F. H. Falcone, S. Stolnik, M. G. Somekh, Journal of Microscopy **231**(1), 68 (2008).
- [28] S. Soria, S. Berneschi, M. Brenci, F. Cosi, G. N. Conti, St. Pelli, G. C. Righini, Sensors **11**, 785 (2011).
- [29] L. Liu, S. Kheifets V. Ginis, A. Di Donato, F. Capasso, PNAS **114**(42), 11087 (2017).